https://dx.doi.org/10.21577/0103-5053.20220115

*J. Braz. Chem. Soc.*, Vol. 34, No. 3, 377-389, 2023


Article

# Metal Oxide Films as Charge Transport Layers for Solution-Processed Polymer Light-Emitting Diodes

*Andreia de Morais*[a] *and Jilian N. de Freitas*[*,a]

[a]*Centro de Tecnologia da Informação Renato Archer (CTI), Rod. D. Pedro I, km 143,6, 13069-901 Campinas-SP, Brazil*

Here, we discuss the use of metal oxide films as charge transport layers in polymer light-emitting diodes containing poly(9,9-dioctyl-9*H*-fluorene-2,7-diyl) (PFO) as emissive layer. A simple device architecture consisting of glass-ITO | poly(3,4-ethylenedioxythiophene)-poly(styrenesulfonate) (PEDOT:PSS) | poly(9-vinylcarbazole) (PVK) | PFO | Ca | Al was used as starting point. This device assembly allows the investigation of basic properties of polymeric emitting layers, but does not provide stable devices with high performances. Thus, a more complex, multilayered diode structure is needed. We pursuit that goal with focus on the use of low-cost, easily processed materials. At one side, solution-processed non-stoichiometric $MoO_x$ films were used to replace the PEDOT:PSS as hole transport layer. At the other interface, solution-processed ZnO films containing either the bare oxide or a ZnO/carbon dots composite were introduced as electron transport layer. By tunning the characteristics of the metal oxide films, the performance of the blue-emitting PFO-based polymer light-emitting diodes (PLEDs) was massively enhanced.

**Keywords:** OLED, PLED, ZnO, $MoO_3$, polyfluorene

## Introduction

Polymer light-emitting diodes (PLEDs) have been the subject of intense research as a class of organic light-emitting diodes that could potentially be prepared from solution processing techniques, with low costs and reduced fabrication complexity, for application in full-color displays or as lighting sources.[1,2] The development of PLEDs is important not only from the technological point of view, but also for the study of electroluminescent phenomena in novel polymers and polymeric composites, thus there is also a giant academic interested associated with these devices.

In lab-scale research, a simple device architecture that can be used for the preparation of PLEDs consists of glass-ITO | PEDOT:PSS | PVK | light-emitting polymer | Ca | Al, in which commercially available materials are used: calcium, aluminum, indium tin oxide (ITO), poly(9-vinylcarbazole) (PVK) and poly(3,4-ethylenedioxythiophene)-poly(styrenesulfonate) (PEDOT:PSS). Although this device assembly allows investigation of the basic properties of different polymeric emitting layers,[3-7] it does not allow to achieve stable devices with high performances. This is related to imbalanced carrier injection and transport due to the lack of an electron transport layer and to degradation mechanisms brough by the use of a hole conductor layer based on PEDOT:PSS. Thus, even for the study of basic electroluminescence principles of PLEDs, a more complex, multilayered diode structure should be used.

Many materials have been investigated in the pursuit of solution-processable, efficient PLEDs. Among them, transition metal oxides have been widely used as charge transport layers in light-emitting diodes[8-10] and solar cells.[11-13] In the hole transport layer (HTL), $MoO_x$ has been considered a promising candidate to replace the frequently used PEDOT:PSS, due to several factors, such as suitable energy level alignment, low contact resistance, non-toxicity, mild deposition temperature, transparency, improvements in the adhesion and morphology of the active layer, and higher stablity.[8,14-16] It has been demonstrated that the tailored work function and appropriate hole injection capacity introduced by this material result in optimized charge carrier balance in light-emitting diodes.[17] Furthermore, the largely used PEDOT:PSS has been pointed as one of the sources of device degradation because of the presence of moisture, since PEDOT:PSS is deposited from aqueous solutions,[18] and because its acidic nature might etch the indium-tin-

*e-mail: jilian.freitas@cti.gov.br
Editor handled this article: Pedro H. C. Camargo (Associate)

oxide (ITO) electrode.[19,20] Both these characteristics affect device durability and shows the urge to find a suitable replacement for PEDOT:PSS in the HTL.

At the other interface, ZnO films have been widely used as electron transport layer (ETL) to improve the electronic transport between the emissive layer and the metallic electrode.[21,22] ZnO has a high electronic mobility, wide energy band gap ($E_g$ = 3.20 eV), high valence band level ($E_{VB}$ = 7.6 eV) and can be easily prepared from inexpensive routes. Since ZnO nanoparticles possess a significant number of surface defects, such as oxygen vacancy that may act as electron trap sites, various modifiers have been adopted to tune the energy level and surface characteristics of ZnO films.[23-25]

Here, we discuss the use of metal oxide films as charge transport layers in PLEDs containing poly(9,9-dioctyl-9*H*-fluorene-2,7-diyl) (PFO) as emissive layer. The goal was to refine the diode architecture whilst working with low-cost, easily prepared, solution-processed materials. We discuss the introduction of metal oxide films in the diodes using as starting point a simple, standard PLED architecture of glass-ITO | PEDOT:PSS | PVK | PFO | Ca | Al, which delivered a luminance (L) of 94 cd $m^{-2}$ at 8 V. At one side, ZnO films containing either the bare oxide or a composite of ZnO and carbon dots (CD) were introduced as ETL. The PLED containing ZnO/CD achieved 552 cd $cm^{-2}$ at 8.0 V, with CIE chromaticity coordinates at (0.147; 0.113) and a turn-on voltage ($V_{ON}$) of 3.6 V-an increase of 32% in relation to the diode containing the pristine ZnO film (L = 418 cd $cm^{-2}$ at 8.0 V, CIE (0.148; 0.132) and $V_{ON}$ of 4.0 V). At the other interface, $MoO_x$ was used to replace PEDOT:PSS as HTL. Solution-processed non-stoichiometric $MoO_x$ films were prepared by a sol-gel method, spin-coated onto ITO substrates and thermally treated at different conditions. The PLED containing the $MoO_x$ film (250 °C), combined with the use of ZnO as ETL, delivered the highest L of 888 cd $m^{-2}$, with a more intense blue color (CIE 0.148; 0.102) and a $V_{ON}$ of 4.2 V. Thus, the luminance of the blue-emitting PFO-based PLEDs was impressively enhanced (ca. one order of magnitude) by using the solution-processed metal oxide films.

## Experimental

### Preparation of ZnO and ZnO/CD films

Zinc acetate dihydrate ((Sigma-Aldrich, São Paulo, Brazil, ≥ 98%) was dissolved in methanol (24 mg $mL^{-1}$) and kept under stirring at 65 °C for 30 min. Then, a methanolic solution of KOH (18 mg $mL^{-1}$) was added over a period of 15 min and the resulting mixture was kept under stirring at 65 °C for 2.5 h. To obtain ZnO nanoparticles, the final dispersion was centrifuged and washed with methanol.

Nitrogen-doped carbon-dots (CD) were synthesized by solid phase pyrolysis.[26] Initially, a mixture of citric acid (Sigma-Aldrich, 99.5%) and dicyandiamide (Sigma-Aldrich, 99%) was heated at 230 °C for 2 h under continuous nitrogen flow. After cooling, the resulting material was dispersed in ethanol in an ultrasonic bath. The removal of large particles was performed by centrifugation and vacuum filtration through a 0.22 μm porous membrane filter. Finally, the solvent was evaporated on a hot plate (120 °C) until a dry powder was obtained. The CD powder was dispersed in a mixture of *n*-butanol, methanol and chloroform and then filtered through a polyvinylidene fluoride (PVDF) filter (Millipore®, 0.45 mm). Finally, the ZnO nanoparticles were dispersed in this mixture via sonication.[21] Another dispersion containing only ZnO was also prepared, in the absence of CDs. Both dispersions were filtered again before use, through a syringe with a PVDF filter (Millipore®, 0.45 mm). ZnO or ZnO/CD films were deposited by spin-coating (5000 rpm, 40 s) on top of the electroluminescent polymer layer and heated to 100 ºC for 10 min, to afford the ETL in PLEDs.

### Preparation of $MoO_x$ films

$MoO_3$ (0.75 g) (Sigma-Aldrich, 99.5%) was dissolved in 5 mL of $H_2O_2$ (at 35%) and refluxed at 80 °C for 2 h (the color of the dispersion turns yellow). The viscosity of the solution was adjusted by addition of polyethylene glycol with molar mass of 600 g $mol^{-1}$ under reflux, at a volume ratio of 1:0.2. Different aliquots of $MoO_x/H_2O_2$/PEG600 were dissolved (from 400 to 800 μL) in 2-methoxyethanol (Sigma-Aldrich, anhydrous, 99.8%), to provide films of different thicknesses. The final volume of each $MoO_x$ solution was 2 mL. Before use, these solutions were filtered through a syringe with a PVDF filter (Millipore®, 0.45 mm). The filtered solution was deposited onto ITO-glass substrates by spin-coating (4000 rpm, 40 s) and heated to varied temperatures (from 150 to 300 ºC), to afford the HTL in PLEDs.

### PLED assembly

#### Substrate patterning

An ITO-glass plate (ITO coated Corning® Eagle XGTM glass, 7-10 ohm $sq^{-1}$, Corning, New York, USA) was cut into pieces of 7.5 cm × 7.5 cm and patterned by photolithography, using the AZ5214 positive photoresist. Wet etching using acidic solution was performed to remove part of the ITO conductive layer and delimit the active area and pixel format of the PLEDs. After removing the

photoresist with acetone, the ITO pieces were cut into smaller sizes (2.5 cm × 1.5 cm), where each piece contained 4 independent diodes with active area of 9 $mm^2$. The patterned ITO substrates were cleaned by sonication in a sequence of acid solution, deionized water and isopropanol, for 7 min each step. After drying under nitrogen flow, an oxygen plasma treatment was applied for 5 min and the substrates were ready for use.

### Standard PLED

A diode with a standard configuration of glass-ITO | PEDOT:PSS | PVK | PFO | Ca | Al, as illustrated in Figure 1a, was assembled as follows. An aqueous solution of PEDOT:PSS (Clevios P VP AI 4083, H.C. Starck, Lewverkusen, Germany) was deposited onto the patterned ITO-glass substrate by spin-coating (3000 rpm, 40 s) and annealed at 150 °C for 15 min on a hot plate, then inserted in a glovebox (MBraun, Garching, Germany) filled with nitrogen. PVK (10 mg $mL^{-1}$ in tetrahydrofuran) and PFO (10 mg $mL^{-1}$ in chlorobenzene) stock solutions were prepared and kept under stirring for 24 h to ensure homogenization. On top of the glass-ITO | PEDOT:PSS, an aliquot of the PVK dispersion was deposited by spin-coating (4000 rpm, 40 s), followed by the deposition of an aliquot of PFO (2000 rpm, 40 s). Then, the film stack was annealed at 100 °C for 10 min on a hot plate. Finally, calcium and aluminum were deposited by thermal evaporation in vacuum (ca. $5 \times 10^{-6}$ mbar).

### PLEDs with ZnO or ZnO/CD ETL

After deposition of the PFO layer, following the same steps described for the standard PLED for the preparation of underneath layers, an additional layer of ZnO or ZnO/CD was deposited by spin-coating (5000 rpm, 40 s) on top of glass-ITO | PEDOT:PSS | PVK | PFO film stack, and then annealed at 100 °C for 10 min on a hot plate. Then, calcium and aluminum were deposited by thermal evaporation, to afford diodes with the configuration of glass-ITO | PEDOT:PSS | PVK | PFO | ZnO or ZnO/CDs | Ca | Al, as illustrated in Figure 1b.

### PLEDs with $MoO_x$ HTL

$MoO_x$ films were deposited onto the patterned ITO-glass by spin-coating (4000 rpm, 40 s) and annealed for 10 min on a hot plate at different temperatures (150, 200, 250 and 300 °C). On top of ITO | $MoO_x$ were deposited the PVK, PFO, ZnO layers, finalizing with thermal evaporation of the calcium and aluminum electrode, following previously described procedures, to afford diodes with the configuration of glass-ITO | $MoO_x$ | PVK | PFO | ZnO | Ca | Al, as illustrated in Figure 1c.

### PLED with $MoO_3$

A diode with the configuration: ITO | $MoO_{3(evap)}$ | PVK | PFO | ZnO | Ca | Al, containing a $MoO_3$ layer deposited by thermal evaporation of $MoO_3$ onto the ITO substrate, instead of the solution-processed $MoO_x$ layer, was also prepared for comparison.

### Characterizations

The films were analyzed with atomic force microscopy (AFM) in a Nanosurf EasysScan 2 microscope (Liestal, Switzerland) operating in the tapping-mode. Film thicknesses

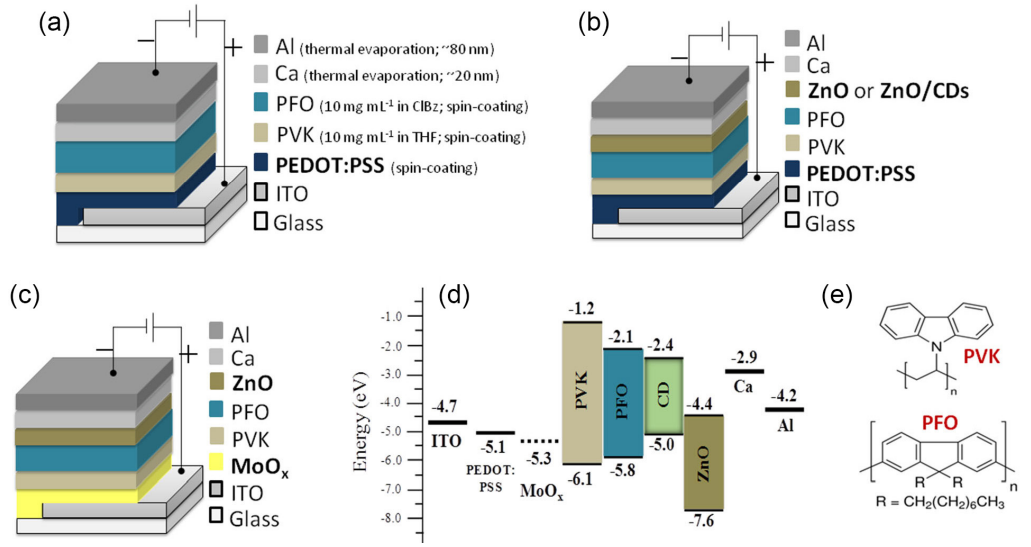


**Figure 1.** (a) Illustration of the layers that compose the standard PLED. (b, c) Illustration of the multilayered PLEDs containing solution-processed metal oxide layers. (d) Diagram showing the energy levels of all materials used in the PLEDs (values of work function, highest occupied molecular orbital (HOMO) and lowest unoccupied molecular orbital (LUMO) were extracted from the literature).[5,27-30] (e) Chemical structure of the polymers PVK and PFO.

were estimated with a DektakXT profilometer (Bruker, Atibaia, Brazil). The PLEDs were characterized by measuring the current density *versus* voltage (J-V) curves with a Keithley Source Meter 2410C (Cole-Parmer, St Neots, UK). The electroluminescence (EL) spectra were collected with a portable Ocean Optics USB2000+ fluorimeter (Orlando, USA). The luminance (L) data and CIE chromatic coordinates were obtained with a Chroma Meter CS-100A equipment (Konica Minolta, New Jersey, USA).

## Results and Discussion

Firstly, a PLED with a standard configuration of glass-ITO | PEDOT:PSS | PVK | PFO | Ca | Al, illustrated in Figure 1a, was assembled using only commercially available materials. The chemical structure of polymers PVK and PFO are shown in Figure 1e. This diode presented a $V_{ON}$ of 4.2 V, L of 94 cd $cm^{-2}$, current density (J) of 0.409 mA $cm^{-2}$, current efficiency ($\eta$) of 22.9 mcd $A^{-1}$ and CIE chromaticity coordinates (0.165, 0.183) at 8 V of applied voltage. This performance is comparable to that found in the literature for a PFO-based PLED with similar device configuration,[31] indicating that it was a valid starting point for the study of the additional layers performed here. Thus, this PLED was used as a standard, reference system in this work. This diode architecture has been widely used for lab-scale research, especially for the screening of novel luminescent materials[3-6,32] due to its simple, low-time consuming assembly procedure. Nevertheless, unbalanced charge injection and charge transport, as well as a rough (and therefore inadequate) morphology at the interfaces introduced by non-ideal contacts might limit those studies as well.

Aiming at developing a multilayered PLED architecture with low-cost, easily prepared materials, the development of solution-processed metal oxides as both ETL and HTL was demonstrated here, using the standard blue-emitting PFO simple structured diode as starting point. At one side of the diode, a solution-processed ZnO layer was added on top of the PFO electroluminescent layer, to act as the ETL. ZnO was spin-cast from a mixture of *n*-butanol, methanol and chloroform. Since the polymer PFO is insoluble in the alcohols used in the mixture, no dissolution (and consequent loss) of the polymeric material was observed in this step. Nevertheless, we cannot discard the possibility that the introduction of ZnO layer could cause changes to the morphology of the underlaying polymeric material, as will be discussed later.

The glass-ITO | PEDOT:PSS | PVK | PFO | ZnO | Ca | Al diode (depicted in Figure 1b) showed an expressive enhancement of the performance in comparison to the standard PLED. Upon introduction of the ZnO ETL, the diode delivered a L of 418 cd $cm^{-2}$, J of 0.620 mA $cm^{-2}$, $\eta$ of 67.4 mcd $A^{-1}$ and chromaticity coordinates of (0.148, 0.132) at 8 V of applied voltage, with a $V_{ON}$ of 4.0 V. In spite of the impressive improvement in brightness, it was found that the surface of the ZnO ETL thus prepared was very rough. AFM analyses in large scan areas of 50 μm × 50 μm (data not shown) revealed that the root mean square (RMS) surface roughness at the film stack (glass-ITO | PEDOT:PSS | PVK | PFO | ZnO) was ca. 39 nm. This represents a significant reduction of roughness in relation to the PFO surface (RMS ca. 63 nm) but is still not smooth enough and could lead to unwanted losses at the ZnO | Ca | Al interface.

To address this issue, the ETL was further tuned by modifying ZnO with CDs. These materials are *quasi*-spherical nanostructures containing carbon atoms with $sp^2$ and $sp^3$ hybridization, and hydrophilic functional groups on their surface. The functional groups are excellent reactive sites for a variety of functionalizations and doping with heteroatoms such as nitrogen, phosphorus and sulfur.[33] It has been reported that nitrogen-doped CDs can act as electron acceptors and transporters when incorporated into thin films of inorganic semiconductors,[14,34] with promising features for light-emitting applications.[35] Lately, several studies have explored the application of CDs in LEDs, where they have been used either as the electroluminescent material, as ETL or as interface modifier.[36] Here, a composite of ZnO-CD was investigated aiming at the use of small concentrations of the carbonaceous material, since it has a more complex synthetic procedure than ZnO, and also to take advantage of the interaction between both materials not only on the surface, but throughout all film extension, since it has been argued that CDs could passivate the defects on the ZnO film.[37] It was also expected that the incorporation of a carbonaceous material would improve the contact between the hydrophilic ZnO and hydrophobic PFO layer.

The diode containing the ZnO-CD composite as ETL (glass-ITO | PEDOT:PSS | PVK | PFO | ZnO-CD | Ca | Al), presented a $V_{ON}$ of 3.6 V, L of 552 cd $cm^{-2}$, J of 0.617 mA $cm^{-2}$, $\eta$ of 89.5 mcd $A^{-1}$ and CIE (0.147, 0.113) at 8 V. Thus, a further enhancement of the PLED properties was obtained by using the ZnO-CD composite, showing that this approach could be used to further tune the device performance. The use of ZnO-CD composite containing 0.1% of CDs, instead of the bare ZnO film, further reduced the surface roughness (RMS ca. 34 nm), thus contributing to the formation of a more favorable interface at the cathode. Furthermore, the incorporation of the CDs in the ETL may facilitate electron injection to PFO, since a lower energy barrier is formed at the interface with this material, as illustrated in the energy level diagram in Figure 1d, thus reducing the turn-on voltage of this PLED. A thorough investigation

of the role of CDs, as well as the effects of tuning the CD concentration in the composites will be reported elsewhere.

Figure 2 displays the J-V, luminance-voltage (L-V) and current efficiency-voltage (η-V) curves, as well as the normalized EL spectra of the PLED assembled with the standard structure, in comparison to the PLEDs containing the ZnO or the ZnO-CD additional ETL layer. It is clearly seen that both L and η are significantly enhanced, while $V_{ON}$ is reduced, thus showing the effective approach of modifying the standard PLED with ZnO or ZnO-CD based ETL. All the EL spectrum exhibited a characteristic vibronic progression with bands centered at 430, 450 and 480 nm, assigned to the 0-0, 0-1, 0-2 singlet exciton transition of the PFO film, indicating the existence of a mixture of the PFO crystalline (β-phase) and amorphous (α-phase) phases. An aggregation signal is also observed at around 520 nm. It is noted that the EL spectra changes after addition of the ETL, with a small enhancement in the relative intensity of the bands centered at 480 and 520 nm, suggesting that the addition of the ETL might be accompanied by some impact on the morphology of the polymeric layer underneath, favoring the formation of aggregates.

At the other interface, the PEDOT:PSS film used as HTL was replaced by non-stoichiometric $MoO_x$ films. One of the main reasons for using $MoO_x$ in organic devices is related to the higher work function of this metal oxide in comparison with PEDOT:PSS, which favors energy alignment at the interface with organic materials. In the energy levels diagram illustrated in Figure 1d, it is possible to see that a higher work function of $MoO_x$ would lead to a lower barrier for charge injection into the PVK. This promotes a better energy level alignment, with band-bending and hole injection capacity, improving charge carrier balance, thus leading to enhanced performance, as has been observed in several reports of OLEDs (small-molecule based devices) and QLEDs (quantum dot-based devices) assembled with $MoO_x$ films deposited by thermal evaporation,[17] sputtering,[38] spin-coating[14,29,39] or blade-coating.[40] It is important to point out that the value displayed for the work function of $MoO_x$ in the diagram of Figure 1d was extracted from a few reports on the literature dealing solution-processed $MoO_x$, used as reference.[28-30] Nevertheless, it has been shown that work function of $MoO_x$ might significantly vary upon temperature annealing,[41,42] oxygen/air exposure,[17,42] and also with film thickness,[14,17]

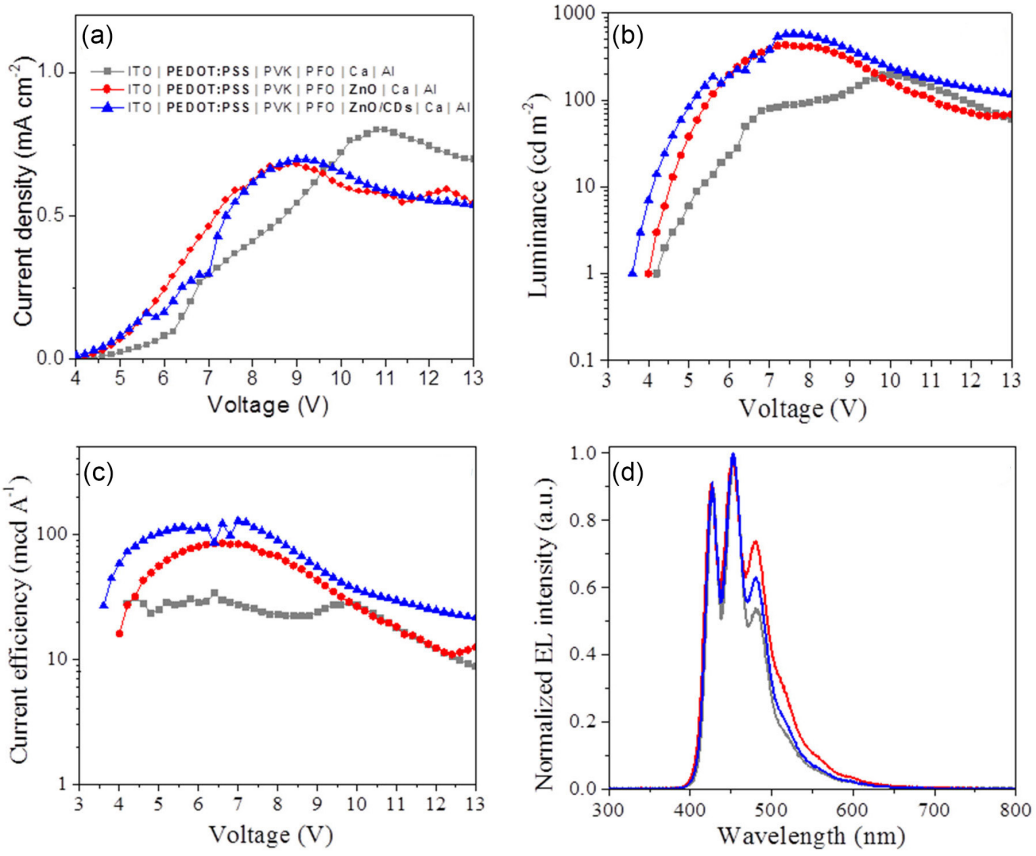


**Figure 2.** (a) Current density, (b) luminance and (c) current efficiency as a function of the applied voltage; and (d) normalized EL spectra (at 8 V) for PLEDs with configuration: (—) glass-ITO | PEDOT:PSS | PVK | PFO | Ca | Al (standard diode), (—) glass-ITO | PEDOT:PSS | PVK | PFO | ZnO | Ca | Al and (—) glass-ITO | PEDOT:PSS | PVK | PFO | ZnO-CD | Ca | Al.

so very different values, ranging from 6.8 eV up to –4.9 eV, have been reported.

In addition, it has been reported that annealing temperatures of at least 275 °C or $O_2$ plasma treatment are required to allow the formation of uniform layers from solution-processing of this material.[9,43,44] Because of the low solubility/dispersivity of $MoO_x$ in solvents, it often results in poor coverage of the substrate and rough morphologies. Thus, the processing conditions needs to be fine-tuned to provide a high-quality $MoO_x$ layer.

To assess this feature, PLEDs were assembled with the configuration glass-ITO | MoOx | PVK | PFO | ZnO | Ca | Al (illustrated in Figure 1c), and the $MoO_x$ films were deposited by spin-coating and submitted to a post-deposition treatment at different annealing temperatures. Figure 3 shows the J-V, L-V and η-V curves and EL spectra obtained for these PLEDs. The parameters extracted from these curves are displayed on Table 1. The PLED containing the $MoO_x$ film annealed at 250 °C for 10 min delivered the highest brightness, achieving L of 888 cd $m^{-2}$ at 10 V, with η of 166.8 mcd $A^{-1}$ and a $V_{ON}$ of 4.2 V. The PLED containing the $MoO_x$ film annealed at 300 °C also showed a reasonable performance, reaching L of 387 cd $m^{-2}$ and η of 243.6 mcd $A^{-1}$ at 10 V, and a $V_{ON}$ of 4.4 V. On the other hand, the films annealed at lower temperatures (200 or 150 °C) did not show a good diode behavior, delivering luminances that were even lower than those of the standard device, and much higher turn-on voltages. The lower temperatures were not sufficient to provide the formation of a smooth, semiconductor film, which could be related to incomplete removal of organic residues from the synthesis and/or a poor interconnection of the nanoparticles. On the other hand, scanning electron microscopy images showed that the $MoO_x$ films annealed at 250 °C are homogeneous and fully cover the substrate (data not shown).

Besides the effect of post-deposition thermal treatment, the effect of varying film thickness was also investigated. Other works have observed thickness dependent performance of thermally deposited $MoO_x$ films in organic devices.[17] It was reported that there is a trade-off between the drift-induced enhancement and increased resistivity of $MoO_x$. The resistance is expected to increase with the thickness of this layer, and an optimal thickness of ca. 20 nm was previously suggested.[17]

Here, the thickness of the $MoO_x$ was varied from 33 to 80 nm (as estimated with a profilometer), which were

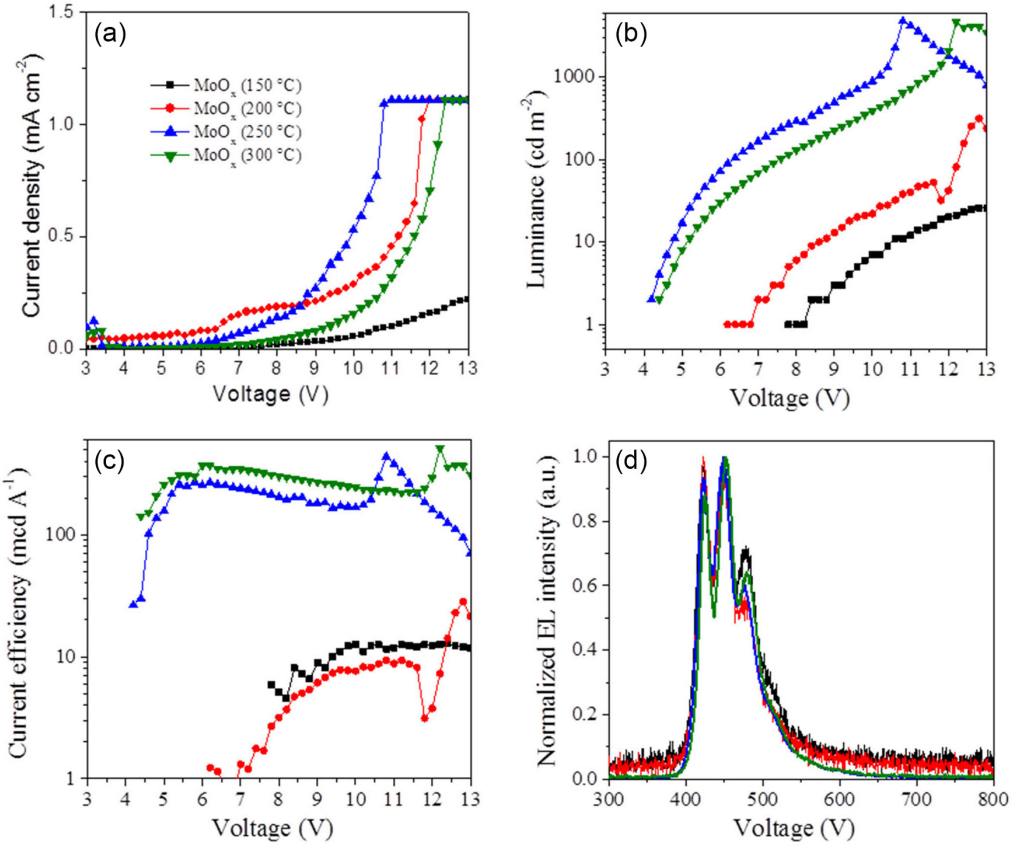


**Figure 3.** (a) Current density, (b) luminance and (c) current efficiency as a function of the applied voltage, and (d) normalized EL spectra (at 10 V) for PLEDs consisting of glass-ITO | $MoO_x$ | PVK | PFO | ZnO | Ca | Al, where the $MoO_x$ films were processed at different temperatures: (—) 150 ºC, (—) 200 ºC, (—) 250 ºC or (—) 300 ºC.

**Table 1.** Parameters obtained for diodes consisting of glass-ITO | $MoO_x$ | PVK | PFO | ZnO | Ca | Al, where the $MoO_x$ films were processed at different temperatures (150, 200, 250 or 300 °C): turn-on voltage ($V_{ON}$), luminance (L), current density (J), current efficiency (η) and CIE chromaticity coordinates. All values, expect $V_{ON}$, were obtained at 10 V of applied voltage

| PLED | $V_{ON}$ / V | L / (cd $m^{-2}$) | J / (mA $cm^{-2}$) | η / (mcd $A^{-1}$) | CIE 1931 (x, y) |
|---|---|---|---|---|---|
| $MoO_x$ (150 °C) | 7.8 | 7 | 0.055 | 12.6 | 0.145, 0.120 |
| $MoO_x$ (200 °C) | 6.2 | 22 | 0.288 | 7.6 | 0.147, 0.095 |
| $MoO_x$ (250 °C) | 4.2 | 888 | 0.532 | 166.8 | 0.148, 0.102 |
| $MoO_x$ (300 °C) | 4.4 | 387 | 0.159 | 243.6 | 0.146, 0.109 |

PLEDs: polymer light-emitting diodes.

obtained by changing from 400 to 800 µL the volume of the aliquot of $MoO_x/H_2O_2$/PEG-600 dissolved in 2-methoxyethanol. The morphology of the films obtained after spin-casting these solutions was investigated by AFM, as shown in Figure 4. The RMS of the film was enhanced from ca. 7 to ca. 14 nm as the aliquot volume was increased from 400 to 800 µL in the precursor solution. The grain size was also enhanced following this trend, with the thickest film (obtained from 800 µL) displaying a rougher, less homogeneous surface. Contrarily, the films obtained from 400 and 500 µL of $MoO_x/H_2O_2$/PEG-600 displayed the most compact and homogenous feature.

For the sake of simplicity, due to numerous experiments and batch runs, PLEDs were prepared without the ZnO ETL, following the standard device architecture, only substituting the PEDOT:PSS for the $MoO_x$ films with varied thickness. The J-V, L-V and η-V curves of the PLEDs consisting of glass-ITO | $MoO_x$ | PVK | PFO | Ca | Al with different $MoO_x$ thickness are displayed in Figure 5, whereas the parameters extracted from these curves are summarized in Table 2.

The data displayed on Table 2 indicates that both L and η were massively enhanced by increasing the $MoO_x$ film thickness. For example, the PLED containing the thinnest $MoO_x$ film delivered L of 179 cd $m^{-2}$ and η of 41.6 mcd $A^{-1}$ (at 10 V), with a $V_{ON}$ of 4.8 V, whereas the PLED containing the thicker $MoO_x$ film achieved L of 1420 cd $m^{-2}$ and η of 175.3 mcd $A^{-1}$ (at 10 V), with a reduced $V_{ON}$ of 4.0 V. At first glance, it seems that there is a positive effect from enhancing the $MoO_x$ film thickness, once much higher brightness and overall performances seem to be achieved with thicker films. However, a careful consideration of EL spectra shown in Figure 5d reveals that changing the $MoO_x$ thickness also caused a massive impact on the EL profile: by enhancing the film thickness, the bands at 480 and 520 nm become more pronounced, even reaching higher intensities than the bands

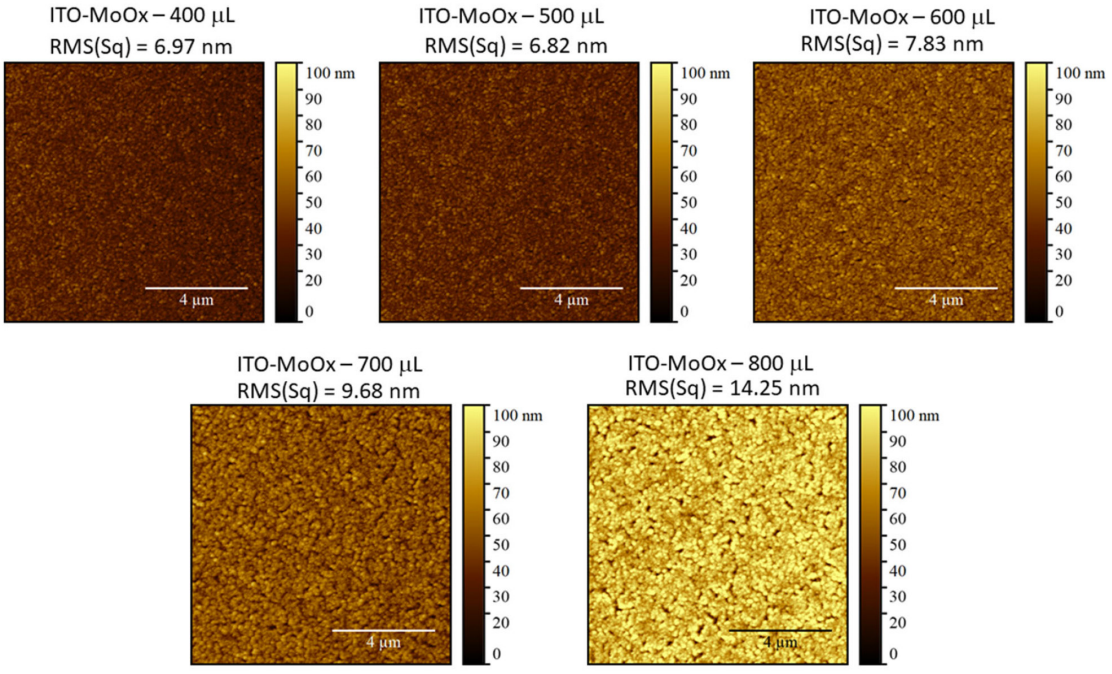


**Figure 4.** AFM images of ITO | $MoO_x$ films spin-coated from precursor solutions containing different aliquots (400 to 800 µL) of $MoO_x/H_2O_2$/PEG-600 in 2-methoxyethanol. The scale bar indicates 4 µm (scan area = 10 µm × 10 µm).

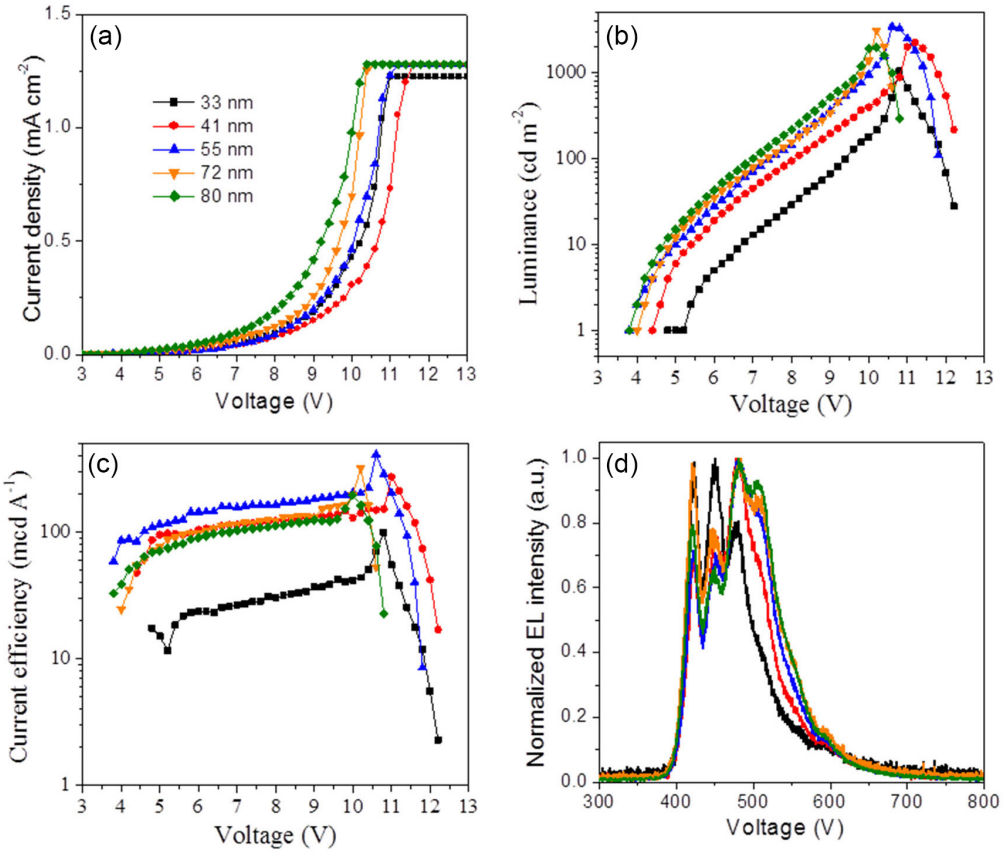


**Figure 5.** (a) Current density, (b) luminance and (c) current efficiency as a function of the applied voltage; and (d) normalized EL spectra (at 10 V) for PLEDs consisting of glass-ITO | $MoO_x$ | PVK | PFO | Ca | Al, for different thicknesses of the $MoO_x$ layer: (—) 33 nm, (—) 41 nm, (—) 55 nm, (—) 72 nm or (—) 80 nm.

**Table 2.** Parameters obtained for diodes containing different thicknesses of the $MoO_x$ layer (glass-ITO | $MoO_x$ | PVK | PFO | Ca | Al): turn-on voltage ($V_{ON}$), luminance (L) and current efficiency (η) obtained at 10 V of applied voltage

| Aliquot volume / μL | Film thickness / nm | $V_{ON}$ / V | L / (cd $m^{-2}$) | η / (mcd $A^{-1}$) | CIE 1931 (x, y) |
|---|---|---|---|---|---|
| 400 | 33 | 4.8 | 179 | 41.6 | 0.159, 0.168 |
| 500 | 41 | 4.4 | 396 | 129.6 | 0.162, 0.234 |
| 600 | 55 | 3.8 | 955 | 206.1 | 0.166, 0.278 |
| 700 | 72 | 4.0 | 1377 | 196.8 | 0.171, 0.277 |
| 800 | 80 | 4.0 | 1420 | 175.3 | 0.171, 0.292 |

at 430 and 450 nm (i.e., there is an inversion in relation to the typical PFO EL spectral profile). This means that, in the conditions investigated here, the green component in the EL spectra dominates the emission of PFO-based diodes prepared with thicker $MoO_x$ layers, in detriment of the blue-light emission in the lower wavelength spectral region. As a general trend, the EL profile already displays a change for the 41 nm film, with further change and inversion of the bands intensity up to 80 nm. All of these PLEDs, with exception of that prepared with the 33 nm-thick $MoO_3$ film, presented an EL with very strong green bands and weak blue emissions, meaning that the blue component was suppressed and green band was enhanced.

The origin of green light emission in the EL spectra of polyfluorenes has been widely debated and is not a settled matter. It is known that an emission signal in the region of 490-550 nm (green light emission) appears in the spectra after ultraviolet light exposure (photooxidation), heating in air (thermal oxidation)[45] or due to the passage of current in the device.[46,47] The origin of this emission has been a subject of strong debate. Some hypothesis are: (*i*) intrachain aggregates of polyfluorene or polyfluorene-based excimer;[48] (*ii*) charge-assisted formation and stabilization of ground-state aggregates;[49] (*iii*) formation of oxidation-induced fluorenone defects with green emission arising from mono-chain fluorenone[50] or fluorenone-based excimer.[51] Even

though the origin of green band in polyfluorenes is not still clear, it is quite often considered undesirable since it causes impurity to the blue emission typically pursuit when PFO is used. On the other hand, it has also been proposed by that one could benefit from this characteristic in order to obtain combined blue and green emissions from a single polymer emissive layer. For example, Ugarte *et al.*[52] suggested that the use of a deliberately oxidized PFO could be combined with red emitting CdSe quantum dots to provide an red, green, blue (RGB) system.

From the results displayed in Figure 4, it is evident that tuning the $MoO_x$ aliquot in the precursor solution, which is translated to enhancements in film thicknesses and changes of morphology and grain sizes after film deposition, leads to the suppression of blue emission and strengthens the green emissions in the PFO-based PLEDs, with high brightness. Whether this effect is caused by a stronger PFO oxidation (due to more defects in thicker $MoO_x$ films, presence of more impurities from the synthesis, or by differences in the work function of $MoO_x$ films of different thicknesses,[14,30] or by a higher current passing through the device because of enhanced charge carrier transport), or by aggregation induced effects (due to changes in the morphology induced by the $MoO_x$ underneath layer, for example), remains an open question. To fully cover that question, a detailed investigation of the electrical characteristics of the $MoO_x$ layer will have to be performed, involving several other techniques, which are out of the scope of the present work and will be addressed elsewhere.

Despite the interesting possibility that one could deliberately take advantage from strong green emission of these systems, since here we were initially aiming at enhancing the characteristic blue emission of PFO-containing PLEDs, the 41 nm thick $MoO_x$ film (obtained from using an intermediary amount of 500 μL of $MoO_x/H_2O_2$/PEG600 dissolved in 2-methoxyethanol) was selected to continue the study. Then, for further evaluation of the $MoO_x$ film, a diode was assembled using an oxide HTL obtained from thermal evaporation of $MoO_3$, with structure: glass-ITO | $MoO_3$ (evap) | PVK | PFO | ZnO | Ca | Al. The thickness of the evaporated film was fixed at 20 nm, following successful results previously described in the literature for thermally deposited $MoO_3$ films.[17] In our case, the diode containing the evaporated $MoO_3$ presented a lower performance in relation to the diode containing $MoO_x$ film (250 °C), reaching only 36 cd $cm^{-2}$ of luminance at 10 V, with J of 0.051 mA $cm^{-2}$, η of 70.1 mcd $A^{-1}$ (10 V) and a $V_{ON}$ of 6.6 V. Since a much higher $V_{ON}$ was obtained in this case, with a poor brightness, one could wonder if the evaporated film of $MoO_3$ did not cover the entire substrate, thus leading to the formation of an inadequate interface at the anode. The J-V, L-V, current efficiency-voltage curves and EL spectra of this diode, as well as the PLED containing the solution-processed $MoO_x$ annealed at 250 °C, and the PLED containing PEDOT:PSS as the HTL, are shown in Figure 6, for comparison.

To further analyze the characteristics of the different HTL investigated here, AFM images of the PEDOT:PSS film, solution-processed $MoO_x$ film (250 °C) and evaporated $MoO_3$ film deposited onto glass-ITO substrates were collected and are displayed in Figure 7. All the films investigated as HTL smoothened the surface of the bare ITO substrate (RMS ca. 10.36 nm). Interestingly, the surface the solution-processed $MoO_x$ film was rougher (RMS ca. 4.03 nm) than the surface of the PEDOT:PSS film (RMS ca. 2.17 nm), in spite of the better results achieved in PLEDs using the former. Interestingly, the lowest roughness among all ETL investigated was obtained with the evaporated $MoO_3$ film. These characteristic rules out the hypothesis of insufficient substrate coverage or inadequate film morphology for this material, and the reason why this material performed poorly in the diodes investigated here must be related to other features.

Regardless of the different surface roughness obtained by changing the HTL material, we note that replacement of the PEDOT:PSS with either $MoO_x$ or evaporated $MoO_3$ showed little impact on the EL spectra of the diode, as can be seen in Figure 6d. Thus, the mechanism by which the $MoO_x$ film enabled the highest diode performance cannot be explained simply by morphology effects on the emissive polymer layer. For OLEDs, QLEDs and PLEDs containing other polymers than the one used here, it has been proposed that incorporation of $MoO_x$ contributes to enhance diode performance through the following ways: reduction of hole-injection barrier due to the high work function of this metal oxide;[10,40,41,53] enhanced hole transport,[54] thus improving charge carrier balance; reduction of the efficiency roll-off typically observed when using PEDOT:PSS;[41] and enhanced operational stability.[30,40,41] A thorough investigation of the electrical and electronic properties of the $MoO_x$ films used in this work to better understand their role in enhancing the PFO-based PLED performance is being conducted and will be reported elsewhere.

Finally, Table 3 summarizes a comparison of the parameters extracted from the optical-electrical characterization of the following PLEDs: standard diode, diodes containing ZnO or ZnO-CD as ETL and PEDOT:PSS as HTL, and the diodes containing ZnO as ETL and $MoO_x$ (250 °C) or $MoO_3$ (evap) as HTL.

From the results displayed on Table 3 it is evidenced that the use of the solution processed oxide layers provided a significant improvement in the performance of PLEDs

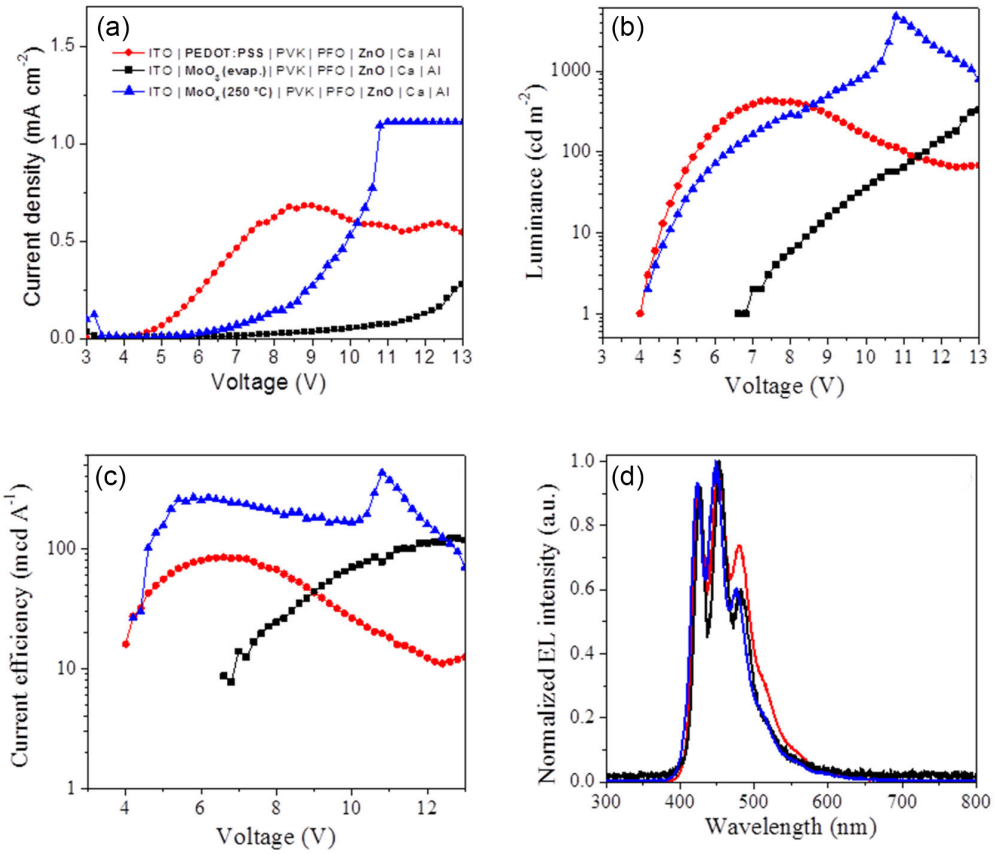


**Figure 6.** (a) Current density, (b) luminance and (c) current efficiency as a function of the applied voltage; and (d) normalized EL spectra for PLEDs with configuration: (—) glass-ITO | PEDOT:PSS | PVK | PFO | ZnO | Ca | Al, (—) glass-ITO | $MoO_3$ (evap.) | PVK | PFO | ZnO | Ca | Al and (—) glass-ITO | $MoO_x$ (250 °C) | PVK | PFO | ZnO | Ca | Al.

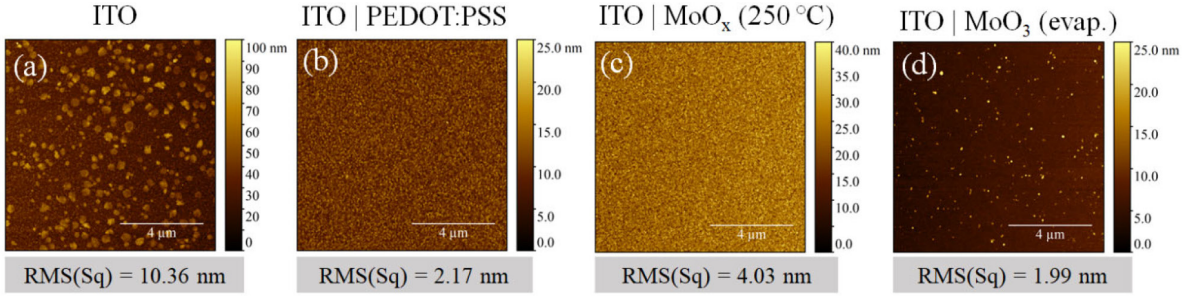


**Figure 7.** AFM images of (a) ITO; (b) ITO | PEDOT:PSS; (c) ITO | $MoO_x$ (250 °C); (d) ITO | $MoO_3$ (evap. ca. 20 nm) films. The scale bar indicates 4 µm (scan area = 10 µm × 10 µm).

**Table 3.** Parameters obtained for diodes containing different materials as HTL and ETL, in comparison with a standard PLED (glass-ITO | PEDOT:PSS | PVK | PFO | Ca | Al): turn-on voltage ($V_{ON}$), luminance (L), current density (J), current efficiency (η) and CIE chromaticity coordinates obtained at 8 V or 10 V of applied voltage (corresponding to the point of maximum brightness)

| HTL | ETL | $V_{ON}$ / V | L / (cd m$^{-2}$) | J / (mA cm$^{-2}$) | η / (mcd A$^{-1}$) | CIE 1931 (x, y) |
|---|---|---|---|---|---|---|
| PEDOT:PSS | [a] | 4.2 | 94 (8 V) | 0.409 (8 V) | 22.9 (8 V) | 0.165, 0.183 |
| PEDOT:PSS | ZnO | 4.0 | 418 (8 V) | 0.620 (8 V) | 67.4 (8 V) | 0.148, 0.132 |
| PEDOT:PSS | ZnO-CD | 3.6 | 552 (8 V) | 0.617 (8 V) | 89.5 (8 V) | 0.147, 0.113 |
| $MoO_x$ (250 °C) | ZnO | 4.2 | 888 (10 V) | 0.532 (10 V) | 166.8 (10 V) | 0.148, 0.102 |
| $MoO_3$ (evap) | ZnO | 6.6 | 36 (10 V) | 0.051 (10 V) | 70.1 (10 V) | 0.144, 0.108 |

[a]Standard PLED without ETL. PEDOT:PSS: poly(3,4-ethylenedioxythiophene)-poly(styrenesulfonate); HTL: hole transport layer; ETL: electron transport layer; CD: carbon dots.

based on PFO as blue-emitting material, because of the drastic enhancement of both L and η. On the other hand, there is some degree of variation on the chromaticity coordinates of the emitted light with the introduction of the metal oxide layers, as can be seen in the CIE diagram displayed in Figure 8. Even at the same condition of applied voltage (8 V), for comparison of the light color emitted by the different diodes, it is possible to see that there is a significant change in the chromaticity coordinates of the PLEDs containing the oxide layers in comparison to the standard diode. A deep, darker blue was obtained using the ZnO and $MoO_x$ optimized layers, which is seen as a positive effect, since it leads towards a purer blue color.

In spite of all the advantages presented here, we note that the optimized post-deposition treatment of $MoO_x$ was performed at 250 °C, meaning that the method investigated here will still require further modification in order be compatible with flexible substrates.

## Conclusions

The assembly of a PLED with a standard configuration of ITO | PEDOT:PSS | PVK | PFO | Ca | Al, based on commercially available materials and using a blue-emitting polyflurorene (PFO) as electroluminescent layer was demonstrated. This simple diode architecture is often used in lab-scale research, especially for the screening of novel materials and for the study of electroluminescence phenomena. The standard PLED delivered a luminance of 94 cd $m^{-2}$ at 8 V of applied voltage, which is a value comparable to that previously reported in the literature. This result was used as a starting point (and comparison basis) for the assembly of more sophisticated, multilayered PLED structures, where the use of metal oxide films as charge transport layers at both interfaces was demonstrated. At one side, ZnO films (containing either the bare oxide or a mixture of ZnO and carbon dots) were introduced to act the electron transport layer. The PLEDs containing ZnO or ZnO/CDs films delivered luminances of 418 and 552 cd $cm^{-2}$ at 8.0 V, respectively, which are over 4 and 5 times higher than that of the standard PLED. At the other interface, solution-processed non-stoichiometric $MoO_x$ films were prepared by a sol-gel method and spin-coated onto ITO substrates, as a replacement for the PEDOT:PSS as a hole transport layer. The PLED containing a ca. 40 μm-thick $MoO_x$ film thermally treated at 250 °C as HTL, and ZnO ETL at the other interface, delivered the highest luminance value, reaching 888 cd $m^{-2}$ at 10 V, which represents an almost one order of magnitude enhancement in relation to the standard PLED. That diode also delivered a current efficiency of 166.8 mcd $A^{-1}$, with a more intense blue color (CIE 0.148, 0.102) at 8.0 V and a $V_{ON}$ of 4.2 V. Both the luminance and current efficiency of the blue-emitting PFO-based diodes were impressively enhanced by using the solution-processed metal oxide films, with no significant impact on the turn-on voltage and slightly changing the chromaticity coordinates of the emitted light to a deeper, darker blue color. Further studies are currently underway to demonstrate the exact role of CDs in ZnO ETL, as well as a further modification of the $MoO_x$ HTL,

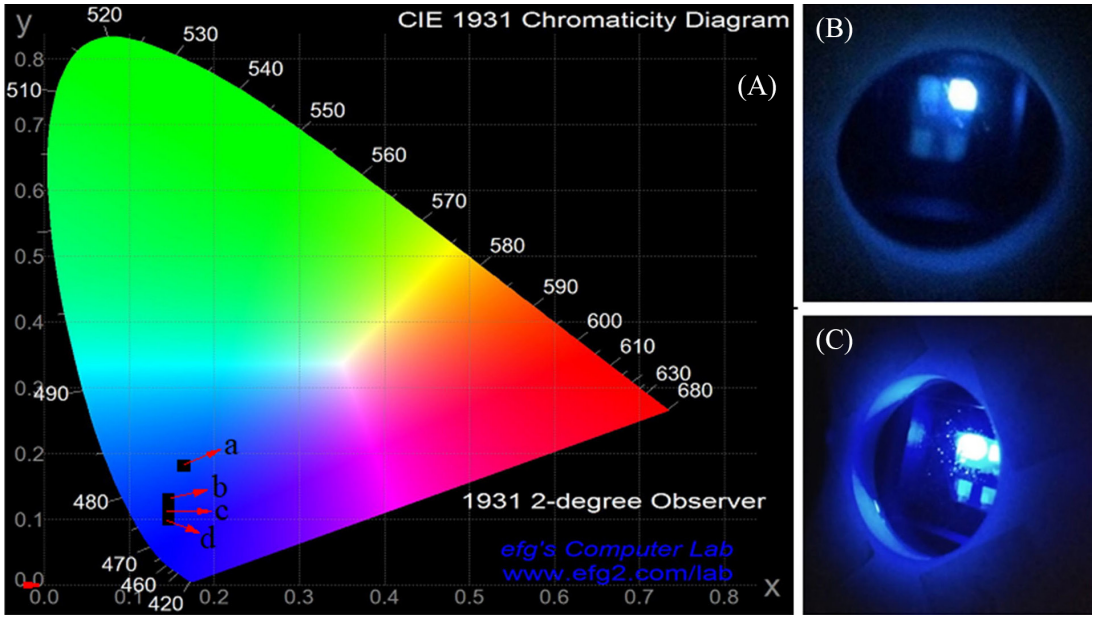


**Figure 8.** (A) CIE chromaticity diagrams of PLEDs at 8 V of applied voltage: (a) glass-ITO | PEDOT:PSS | PVK | PFO | Ca | Al (standard diode), (b) glass-ITO | PEDOT:PSS | PVK | PFO | ZnO | Ca | Al, (c) glass-ITO | PEDOT:PSS | PVK | PFO | ZnO-CD | Ca | Al and (d) glass-ITO | $MoO_x$ (250 °C) | PVK | PFO | ZnO | Ca | Al. Photography of the standard PLED (B) and the PLED containing the optimized $MoO_x$ film as HTL and ZnO as ETL (C).

as will be published elsewhere. The results presented here demonstrate a simple route using low-cost materials to develop a platform for the assembly of PLEDs in glass substrates, which could be easily adopted for the study of different electroluminescent materials.

## Acknowledgments

The authors acknowledge financial support from CNPq and PCI/CTI/CNPq (313069/2016-6 and 301118/2021-3). Research supported by CTI-Nano, strategic laboratory from SisNano, MCTI and financed by CNPq.

## References

1. Inamuddin, I.; Boddula, R.; Ahamed, M. I.; Asiri, A. M.; *Polymers for Light-Emitting Devices and Displays*, 1st ed.; Wiley: New Jersey, USA, 2020.
2. Low, J. Y.; Merican, Z. M. A.; Hamza, M. F.; *Mater. Today: Proc.* **2019**, *16*, 1909. [Crossref]
3. Morais, A.; Bernardo, D. R.; Gemino, J. C.; Nogueira, A. F.; Freitas, J. N.; *J. Lumin.* **2021**, *230*, 117764. [Crossref]
4. Turchetti, D. A.; Domingues, R. A.; Freitas, J. N.; Azevedo, D.; Duarte, L. G. T. A.; Germino, J. C.; Atvars, T. D. Z.; Akcelrud, L. C.; *J. Lumin.* **2018**, *201*, 290. [Crossref]
5. Duarte, L. G. T. A.; Germino, J. C.; Mendes, R. A.; Berbigier, J. F.; Moreira, K. S.; Faleiros, M. M.; de Freitas, J. N.; Burgo, T. A. L.; Rodembusch, F. S.; Atvars, T. D. Z.; *J. Phys. Chem. C* **2020**, *124*, 21036. [Crossref]
6. Germino, J. C.; de Freitas, J. N.; Domingues, R. A.; Quites, F. J.; Faleiros, M. M.; Atvars, T. D. Z.; *Synth. Met.* **2018**, *241*, 7. [Crossref]
7. de Azevedo, D.; Freitas, J. N.; Domingues, R. A.; Faleiros, M. M.; Atvars, T. D. Z.; *Synth. Met.* **2017**, *233*, 28. [Crossref]
8. Huh, Y. H.; Kwon, O. E.; Park, B.; *Opt. Express* **2015**, *23*, A625. [Crossref]
9. Meyer, J.; Hamwi, S.; Kroger, M.; Kowalsky, W.; Riedl, T.; Kahn, A.; *Adv. Mater.* **2012**, *24*, 5408. [Crossref]
10. Zhang, D.-D.; Wang, R.; Ma, Y.-Y.; Wei, H.-X.; Ou, Q. D.; Wang, Q. K.; Zhou, L.; Lee, S. T.; Li, Y. Q.; Tang, J.-X.; *Org. Electron* **2014**, *15*, 961. [Crossref]
11. Girotto, C.; Voroshazi, E.; Cheyns, D.; Heremans, P.; Rand, B. P.; *ACS Appl. Mater. Interfaces* **2011**, *3*, 3244. [Crossref]
12. Kang, Q.; Yang, B.; Xu, Y.; Xu, B.; Hou, J.; *Adv. Mater.* **2018**, *30*, 1801718. [Crossref]
13. Cominetti, A.; Serrano, G.; Savoini, A.; Carbonera, C.; Melchiorre, F.; Perucchini, S.; Congiu, A.; Corso, G.; Barbieri, R.; Trippodo, E.; Caneschi, A.; Po, R.; *Phys. Status Solidi A* **2020**, *217*, 1901023. [Crossref]
14. Zhang, X.; You, F.; Zheng, Q.; Zhang, Z.; Cai, P.; Xue, X.; Xiong, J.; Zhang, J.; *Org. Electron.* **2016**, *39*, 43. [Crossref]
15. Chen, L.; Wang, P.; Li, F.; Yu, S.; Chen, Y.; *Sol. Energy Mater. Sol. Cells* **2012**, *102*, 66. [Crossref]
16. Xu, M.-F.; Cui, L.-S.; Zhu, X.-Z.; Gao, C.-H.; Shi, X.-B.; Jin, Z.-M.; Wang, Z.-K.; Liao, L.-S.; *Org. Electron.* **2013**, *14*, 657. [Crossref]
17. Irfan, I.; Ding, H.; So, F.; Gao, Y.; *J. Photonics Energy* **2011**, 011105-1. [Crossref]
18. So, F.; Kondakov, D.; *Adv. Mater.* **2010**, *22*, 3762. [Crossref]
19. de Jong, M. P.; van Jendoorn, L. J.; de Voigt, M. J. A.; *Appl. Phys. Lett.* **2000**, *77*, 2255. [Crossref]
20. Wong, K. W.; Yip, H. L.; Luo, Y.; Wong, K. Y.; Lau, W. M.; Low, K. H.; Chow, H. F.; Gao, Z. Q.; Yeung, W. L.; Chang, C. C.; *Appl. Phys. Lett.* **2002**, *80*, 2788. [Crossref]
21. Kwak, K.; Cho, K.; Kim, S.; *Phys. Status Solidi C* **2014**, *11*, 234. [Crossref]
22. Zhao, X.-D.; Li, Y.-Q.; Xiang, H.-Y.; Zhang, Y.-B.; Chen, J.-D.; Xu, L.-H.; Tang, J.-X.; *ACS Appl. Mater. Interfaces* **2017**, *9*, 2767. [Crossref]
23. Kim, K.; Suh, M.; Choi, J.; Lee, D.; Kim, Y.; Cheong, S. H.; Kim, D.; Jeon, D. Y.; *Adv. Funct. Mater.* **2015**, *25*, 7450. [Crossref]
24. Park, J. S.; Lee, J. M.; Hwang, S. K.; Lee, S. H.; Lee, H. J.; Lee, B. R.; Park, H. II; Kim, J. S.; Yoo, S.; Song, M. H.; Kim, S. O.; *J. Mater. Chem.* **2012**, *22*, 12695. [Crossref]
25. Son, D. I.; Kwon, B. W.; Park, D. H.; Seo, W. S.; Yi, Y.; Angadi, B.; Lee, C. L.; Choi, W. K.; *Nat. Nanotechnol.* **2012**, *7*, 465. [Crossref]
26. Hou, J.; Wang, W.; Zhou, T.; Wang, B.; Li, H.; Ding, L.; *Nanoscale* **2016**, *8*, 11185. [Crossref]
27. Skriver, H. L.; Rosengaard, N. M.; *Phys. Rev. B* **1992**, *46*, 7157. [Crossref]
28. Zheng, Q.; You, F.; Xu, J.; Xong, J.; Xue, X.; Cai, P.; Zhang, X.; Wang, H.; Wei, B.; Wang, L.; *Org. Electron.* **2017**, *46*, 7. [Crossref]
29. Li, X.; Xie, F.; Zhang, S.; Hou, J.; Choy, W. C. H.; *Light: Sci. Appl.* **2015**, *4*, e273. [Crossref]
30. Alehdaghi, H.; Marandi, M.; Irajizad, A.; Taghavinia, N.; Jang, J.; Zare, H.; *Mater. Chem. Phys.* **2018**, *204*, 262. [Crossref]
31. Stewart, J. S.; Lippert, T.; Nagel, M.; Nuesch, F.; Wokaun, A.; *Appl. Physs. Lett.* **2012**, *100*, 203303. [Crossref]
32. de Azevedo, D.; Freitas, J. N.; Domingues, R. A.; Faleiros, M. M.; Santos, T. E. A.; Atvars, T. D. Z.; *Synth. Met.* **2016**, *222*, 205. [Crossref]
33. Lim, S. Y.; Shen, W.; Gao, Z.; *Chem. Soc. Rev.* **2015**, *44*, 362. [Crossref]
34. Zubair, M.; Mustafa, M.; Ali, A.; Doh, Y. H.; Choi, K. H.; *J. Mater. Sci.: Mater. Electron.* **2015**, *26*, 3344. [Crossref]
35. Li, X.; Rui, M.; Song, J.; Shen, Z.; Zeng, H.; *Adv. Funct. Mater.* **2015**, *25*, 4929. [Crossref]
36. Lagonegro, P.; Giovanella, U.; Pasini, M.; *Coatings* **2021**, *11*, 5. [Crossref]

37. Zhang, X.; Zeng, Q.; Xiong, Y.; Ji, T.; Wang, C.; Shen, X.; Lu, M.; Wang, H.; Wen, S.; Zhang, Y.; Yang, X.; Ge, X.; Zhang, W.; Litvin, A. P.; Baranov, A. V.; Yao, D.; Zhang, H.; Yang, B.; Rogach, A. L.; Zheng, W.; *Adv. Funct. Mater.* **2020**, *30*, 1910530. [Crossref]
38. Liu, L.; Yu, H.; Wang, H.; Zheng, Q.; Zhang, X.; Li, W.; Zhang, Y.; Zhang, X.; Wei, B.; *Phys. Status Solidi A* **2018**, *215*, 1800166. [Crossref]
39. Vu, H.-T.; Su, Y.-K.; Chiang, R.-K.; Huang, C.-Y.; Chen, C.-J.; Yu, H.-C.; *IEEE Photonics Techol. Lett.* **2016**, *28*, 2156. [Crossref]
40. Zeng, Q.; Xu, Z.; Zheng, C.; Liu, Y.; Chen, W.; Guo, T; Li F.; Xiang, C.; Yang, Y.; Cao, W.; Xie, X.; Yan, X.; Qian, L.; Holloway, P. H.; *ACS Appl. Mater. Interfaces* **2018**, *10*, 8258. [Crossref]
41. Li, J.; Guo, Q.; Jin, H.; Wang, K.; Xu, D.; Xu, G.; Xu, X.; *RSC Adv.* **2017**, *7*, 27464. [Crossref]
42. Irfan, I.; Gao, Y.; *J. Photonics Energy* **2012**, 021213-1. [Crossref]
43. Meyer, J.; Khalandovsky, R.; Gorrn, P.; Kahn, A.; *Adv. Mater* **2011**, *23*, 70. [Crossref]
44. Sun, J.-Y.; Tseng, W.-H.; Lan, S.; Lin, S.-H.; Yang, P.-C.; Wu, C.-I.; Lin, C.-F.; *Sol. Energy Mater. Sol. Cells* **2013**, *109*, 178. [Crossref]
45. List, E. J. W.; Gaal, M.; Guentner, R.; de Freitas, P. S.; Scherf, U.; *Synth. Met.* **2003**, *139*, 759. [Crossref]
46. Ouisse, T.; Stephan, O.; Armand, M.; *EPJ Appl. Phys.* **2003**, *24*, 195. [Crossref]
47. Ugarte, I.; Cambarau, W.; Waldauf, C.; Arbeloa, F. L.; Pacios, R.; *Org. Electron*. **2009**, *10*, 1606. [Crossref]
48. Nakamura, T.; Sharma, D. K.; Hirata, S.; Vacha, M.; *J. Phys. Chem. C* **2018**, *122*, 8137. [Crossref]
49. Honmou, Y.; Hirata, S.; Komiyama, H.; Hiyoshi, J.; Kawauchi, S.; Iyoda, T.; Vacha, M.; *Nat. Commun*. **2014**, *5*, 4666. [Crossref]
50. He, B.; Li, J.; Bo, Z.; Huang, Y.; *Polym. J.* **2007**, *39*, 1345. [Crossref]
51. Sims, M.; Bradley, D. D. C.; Ariu, M.; Koeberg, M.; Asimakis, A.; Grell, M.; Lidzey, D. G.; *Adv. Funct. Mater.* **2004**, *14*, 765. [Crossref]
52. Ugarte, I.; Castelló, I.; Palomares, E.; Pacios, E. In *Quantum Dots - A Variety of New Applications*, 1st ed.; Al-Ahmadi, A., ed.; IntechOpen, 2012, p. 115.
53. Zheng, Q.; Qu, D.; Zhang, Y.; Li, W.; Xiong, J.; Cai, P.; Xue, X.; Liu, L.; Wang, H.; Zhang, X.; *Opt. Laser Technnol.* **2018**, *101*, 85. [Crossref]
54. Qiao, X.; Chen, J.; Li, X.; Ma, D.; *J. Appl. Phys.* **2010**, *107*, 104505. [Crossref]

*Submitted: March 11, 2022*
*Published online: August 30, 2022*